Discrete Layer Jamming for Variable Stiffness Co-Robot Arms

Yitong Zhou
Graduate Research Associate
Department of Mechanical and Aerospace Engineering
The Ohio State University
Columbus, Ohio 43210
Email: zhou.1455@osu.edu

Leon M. Headings
Senior Research Associate
Department of Mechanical and Aerospace Engineering
The Ohio State University
Columbus, Ohio 43210
Email: headings.4@osu.edu

Marcelo J. Dapino*
Professor, Fellow of ASME
Department of Mechanical and Aerospace Engineering
The Ohio State University
Columbus, Ohio 43210
Email: dapino.1@osu.edu

Continuous layer jamming is an effective tunable stiffness mechanism that utilizes vacuum to vary friction between laminates enclosed in a membrane. In this paper, we present a discrete layer jamming mechanism that is composed of a multi-layered beam and multiple variable pressure clamps placed discretely along the beam; system stiffness can be varied by changing the pressure applied by the clamps. In comparison to continuous layer jamming, discrete layer jamming offers advantages of simplicity with implementation of dynamic variable pressure actuators for faster control, better portability, and no sealing issues due to no need for air supply. Design and experiments show that discrete layer jamming can be used for a variable stiffness co-robot arm. The concept is validated by quasi-static cantilever bending experiments. The measurements show that clamping 10% of the beam area with two clamps increases bending stiffness by around 17 times when increasing the clamping pressure from 0 to 3 MPa. Computational case studies using finite element analysis for 5 key parameters are presented, including clamp location, clamp width, number of laminates, friction coefficient, and number of clamps. Clamp location, number of clamps, and number of laminates are found to be most useful for optimizing a discrete layer jamming design. Actuation requirements for a variable pressure clamp are presented based on results from laminate beam compression tests.

*Address all correspondence to this author.

1 Introduction

Co-robots work collaboratively with human partners in various kinds of contexts including wearable haptic devices [1], rehabilitation [2, 3], and flexible production lines [4]. In contrast to conventional caged robots which are isolated completely from humans to avoid injury, co-robots are developed to work in a human-involved environment. Therefore, both performance and safety are critical aspects of co-robot design.

Stiff robot arms lead to high injury severity when there is an impact between a robot and an operator. Intentionally introducing compliance to the mechanical design increases the safety of robots [5]. A number of studies focus on embedding variable stiffness actuators (VSA) in robot joints (VSJ) [6, 7, 8, 9]. Recent studies investigated variable stiffness link (VSL) robots [10, 11]. Although VSL is not expected to replace VSJ, Yu et al. stated that the VSL solution could result in a slightly smaller impact force than the VSJ solution [12]. In this paper, we focus on variable stiffness links rather than joints. Therefore, methods to efficiently alter and control the stiffness of robot arms are necessary for designing safe, high performance robotic systems.

Jamming is an effective tunable stiffness method in terms of varying area moment of inertia, among which both granular and layer jamming have been studied for use in robots. By applying constraint force/pressure to an enclosed flexible membrane containing granular or laminar materials, frictional coupling is introduced to the structure, resulting in an increase in area moment of inertia. Granular jamming

has been used in robotic applications such as gripping [13], hyper-redundant manipulators [14], and robotic spines [15]. By applying vacuum to granular materials, such as small pellets or spheres, in a flexible membrane, the granular material can be transitioned between liquid-like and solid-like states, thus achieving tunable stiffness. However, a substantial volume is required to achieve sufficient stiffness for robotic manipulator use, which can result in a bulky system.

The mechanical concept behind layer jamming is the utilization of friction created between flexible laminates to transition between an unjammed, deformable state and a jammed state with solid-like rigidity. The layers are brought into surface contact by applying a jamming force. Various approaches have been used to generate the jamming force. Tabata et al. [16] used stacked flexible polyimide thin films with patterned Ni electrodes to which large positive and negative voltages were applied to generate electrostatic attractive forces between the films. This method requires dangerously high voltages (up to 750 V), and the stiffness change of 4 times may be insufficient for variable stiffness robots. Henke et al. [17] proposed a design with SMA wires surrounding a multi-layered beam. By heating the wires above their transition temperature, the wires contract to compress the layers together, hence increasing stiffness. However, the speed and strength of SMA wires can limit the application, and the outer surface can be dangerous if high SMA transition temperatures are involved. Recent studies have applied vacuum to jam laminates for applications such as human-computer interaction interfaces [18], and robotic applications such as continuum robots [19], minimally invasive surgery robots [20], robot fingers [21], wearable robots [22], and grippers [23]. However, the outer thin membranes that surround the layers can be easily damaged by unintentional contact with rough edges.

In this paper, we propose a tunable stiffness mechanism termed "discrete layer jamming," which employs friction between layers with jamming forces applied by variable pressure clamps located discretely along a multilayer beam. By increasing the clamping force, the beam bending stiffness is increased. Conceptually, the clamping actuation can be achieved with smart materials. Due to their solid state operation, smart materials provide compact and reliable operation involving few to no moving parts and fast dynamic response. The proposed mechanism can be adopted to the end link connecting the end effector or multiple links for serial industrial co-robot manipulators. A preliminary introduction of this mechanism is published in [24], and more detailed and comprehensive study and analysis of its properties are presented herein as a journal article for the first time. In this paper, the proposed discrete layer jamming principle is presented along with computational (FE) modeling, analysis, and supporting experiments. The paper is organized as follows: concept, experiments, and finite element analysis of discrete layer jamming are presented in Section 2; Section 3 shows computational parametric studies; Section 4 describes the testing of multi-layered beams and the actuation requirements for a variable pressure actuator; conclusions and future work are provided in Section 5.

2 Design and Analysis of Discrete Layer Jamming

2.1 Continuous Layer Jamming Concept

The concept of continuous layer jamming for a multilayer beam with a point load at the end is demonstrated in Fig. 1, where Fig. 1(a) and Fig. 1(b) illustrate the unjammed state which has no external jamming force, and a jammed state with jamming force, respectively. Without a jamming force, each laminate deflects nearly independently. Applying a jamming force provides friction coupling between the laminates to resist sliding between laminates, hence increasing stiffness. For a pneumatic continuous layer jamming system, the jamming force is provided by the vacuum pressure to an enclosed membrane containing the layers, as shown in [20]. Multiple references have pointed out that continuous layer jamming can theoretically achieve a stiffness change of n^2, where n is the number of layers [17, 25]. Hence a 10-layered beam can ideally achieve a 100 times stiffness change. However, pneumatic continuous jamming is limited by actuation speed which can be insufficient for certain robotic control requirements.

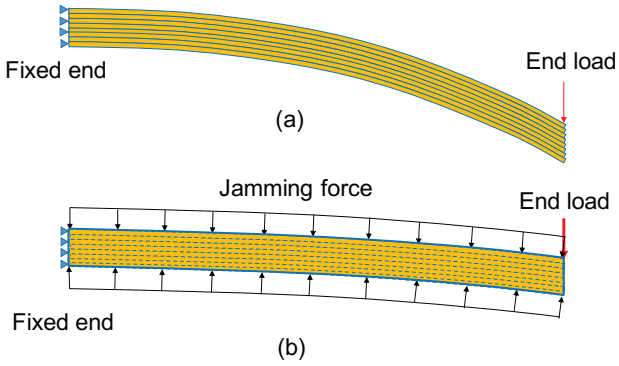

Fig. 1 : Concept of continuous layer jamming. (a) Unjammed state. (b) Jammed state.

2.2 Discrete Layer Jamming Concept

Instead of using a pneumatic source to jam the laminates continuously along the beam, we propose to use variable pressure clamps to apply the jamming force, as shown in Fig. 2. Beam stiffness can be varied by changing pressure applied by the clamps. For illustration purposes, the structure has two clamps placed near the middle and end of the beam. We define n as the number of laminates and t as the laminate thickness. Beam width, length, and total thickness are W, L, and $T(=nt)$, respectively. The clamp near the middle divides the beam length into two segments with lengths of L_1 and L_2. Pressure P_i is applied to the beam by the ith clamp with a width of C_i. Therefore, the clamping force F_i applied to the ith clamp can be expressed by:

$$F_i = P_i C_i W \tag{1}$$

Defining μ as the friction coefficient, the friction force in the ith clamp region between all layers is simply:

$$f_i = (n-1)\mu F_i \tag{2}$$

The friction force generated from N clamps can be summed as:

$$f = \sum_{i=1}^{N} (n-1)\mu F_i = \sum_{i=1}^{N} (n-1)\mu P_i C_i W, \qquad (3)$$

which indicates that the friction force increases with the number of clamps, the number of laminates, the friction coefficient, the clamp pressure, and the clamp size. Therefore, for a system with fixed number of clamps, number of laminates, clamp size, and friction coefficient, system stiffness can be varied by changing the clamp pressure.

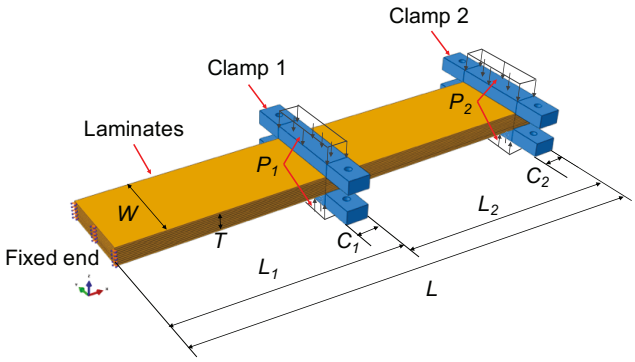

Fig. 2 : Proposed concept of discrete layer jamming.

2.3 Experimental Setup

In its simplest form, a discrete layer jamming structure needs to include only some laminate material and one or more clamps. To prove the concept of a discrete layer jamming structure with variable stiffness, a stack was fabricated with 10 ABS layers, each 1.59 mm thick, 70 mm wide, and 400 mm long. This yields a 15.9 mm thick beam in non-clamped regions. The laminates were laser cut from ABS sheets to create the desired shape. We selected ABS for the prototype material due to its relatively high flexibility and elasticity to achieve sufficient stiffness change. To apply uniform clamping pressure, two identical frame clamps were designed and manufactured from aluminum, as shown in Fig. 3. Both clamps have a width of 20 mm. An Omega LC703-1k load cell was embedded in each frame clamp. A pressure adjustment bolt is connected to the pressing block, which presses the load cell attached to the pressing plate which clamps the layers. By tightening the pressure adjustment bolt, the compression force applied by the clamps can be increased.

To investigate the relationship between bending stiffness and pressure applied by the clamps, we conducted quasi-static cantilever bending experiments for various pressure states, as shown in Fig. 4 (a). Two clamps are placed 180 mm and 380 mm respectively from the fixed end of the beam. In order to denote the clamp location more specifically, we name the clamp near the middle of the beam as the middle clamp and the clamp near the end as the end clamp. The clamping force applied by each clamp was measured by the load cell with a Vishay signal conditioning amplifier and recorded by a Quattro data acquisition system (DAQ). A

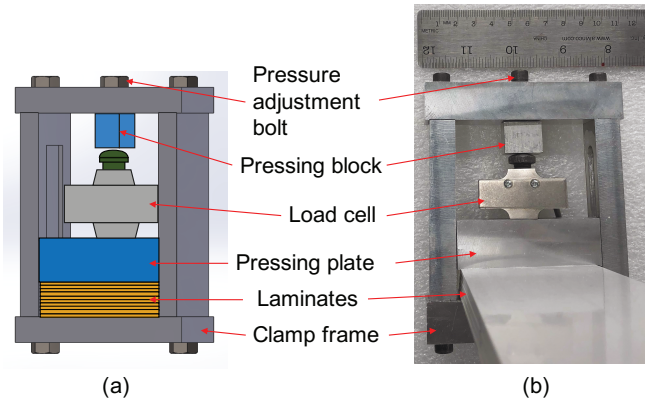

Fig. 3 : (a) Clamp design. (b) Clamp prototype.

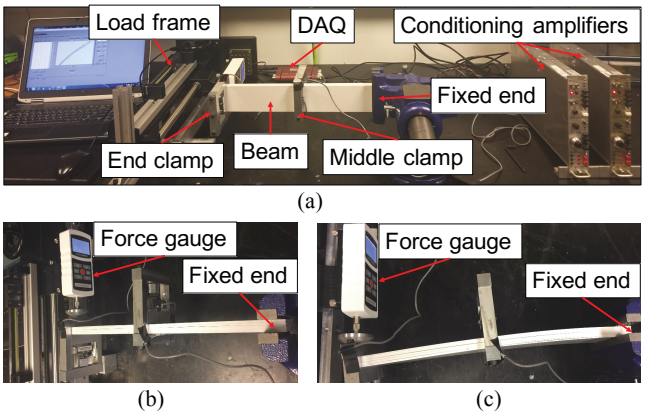

Fig. 4 : Cantilever bending test setup. (a) Test setup. (b) Top view of initial state. (c) Top view of deflected state.

Mark-10 ES30 load frame was used to apply a tip load to the free end of the prototype beam structure. A Mark-10 ME-200 force gauge was used to measure the tip load. Initial and deflected shapes of the beam structure are demonstrated in Fig. 4(b) and Fig. 4(c), respectively. Experimental specifications are shown in Table 1.

Table 1 : Experimental specifications.

Symbol	Specification	Value
W	Laminate width	70 mm
t	Laminate thickness	1.59 mm (1/16 in)
T	Total thickness of beam	15.9 mm
L_i	ith segment length	200 mm, $i = 1,2$
L	Beam length	400 mm
C_i	ith clamp width	20 mm, $i = 1,2$
n	Number of laminates	10
N	Number of clamps	2
μ	Friction coefficient	0.6
D	End deflection	40 mm
P_i	Pressure of ith clamp	0, 0.05, 0.5, 1, 3 MPa
Y	Young's modulus	2.2 GPa

2.4 Test Procedures

The pressures applied to clamps 1 and 2 were 0, 0.05, 0.5, 1, and 3 MPa, which resulted in 25 pressure combinations. Zero pressure represents the state of no clamps or pressure in this paper. We conducted one cantilever bending test for each pressure state over three displacement cycles. For each test, we applied 40 mm tip deflection, which is 10% of the cantilever beam length. For abbreviated notation of the different pressure cases, "M" and "E" indicate the mid-

dle clamp pressure and the end clamp pressure, respectively. Here, we use the unit of pressure MPa. For instance, M3E0 represents a middle clamp pressure of 3 MPa and no end clamp pressure (clamp and pressure free). M0E0 indicates no clamps or pressures, which is the unjammed state.

2.5 Experimental Results and Discussion

The deflected shapes of 9 out of 25 pressure states are shown in Fig. 5. When comparing M0.05E3 in Fig. 5(b) and M3E0.05 in Fig. 5(d), it is observed that with the same tip deflection of 40 mm, M0.05E3 deflects more in the first segment, whereas M3E0.05 deflects more in the second segment. In addition, the higher the clamping pressure, the flatter the slope near the clamping area.

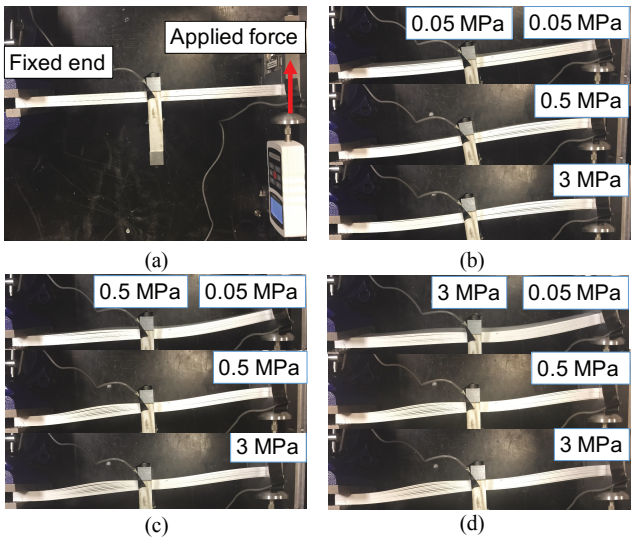

Fig. 5 : (a) Initial state. Deflected shapes of nine pressure states: (b) M0.05E0.05, M0.05E0.5, and M0.05E3; (c) M0.5E0.05, M0.5E0.5, and M0.5E3; (d) M3E0.05, M3E0.5, and M3E3.

Fig. 6(a) and Fig. 6(b) show force-displacement curves of M0 and M3 pressure states, respectively, with end clamp pressures of 0, 0.05, 0.5, 1, and 3 MPa. It is observed that both figures show similar slopes at very small deflections, which suggests that the stiffness does not depend on the clamp pressure. The stiffnesses are independent because laminates are initially sticking for all pressure cases. Once the shear force between the individual laminates is large enough to overcome the static friction limit, which varies according to the clamping pressure, the laminates begin to slide against each other and the force-displacement curves become nonlinear. Below this limit, the layers are effectively jammed and the curves are relatively linear. M3E0.5, M3E1, and M3E3 curves in Fig. 6(b) almost overlap with each other, which indicates similar stiffnesses. A wavy behavior is found in the M0E0.05 curve at large deflections in Fig. 6(a) and the M3E0.05 curve in Fig. 6(b) demonstrates a drop, which both indicate slipping between the laminates. Compared to the M0 curves in Fig. 6(a), M3 curves in Fig. 6(b) tend to be smoother. The reason is that the resolution of the Mark-10 ME-200 force gauge is 0.1 N, so measurement noise is more evident for the M0 series compared to the M3 series. In addition, we observed hysteresis in all pressures investigated except M0E0, but found higher hysteresis in lower pressure states such as M0.05E0.05. Hysteresis is likely due to slipping between the laminates. The lower the pressure, the more slipping, and the higher the hysteresis. The M0E0 pressure state has no clamps or pressure so laminates can freely slide back during unloading, hence no hysteresis.

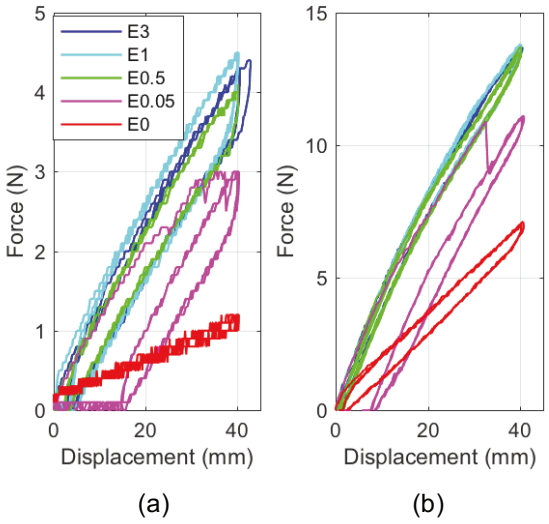

Fig. 6 : Measured force-displacement curves from cantilever bending tests of (a) M0 series, and (b) M3 series.

To study the effects of clamp pressure on bending stiffness, we obtained stiffness as the slope of the line fitted to the first 20 mm of each force-displacement curve. The stiffnesses for all 25 pressure states are summarized in Table 2. Here, we found the maximum stiffness to be 0.41 N/mm at M3E1 and the minimum stiffness to be 0.024 N/mm at M0E0. We define the stiffness of some pressure state as k_p, the minimum stiffness as k_{min}, the maximum stiffness as k_{max}, and stiffness ratio as k_p/k_{min}. We then define the maximum stiffness ratio as $K_r = k_{max}/k_{min}$.

Therefore, the maximum stiffness ratio is found to be around 17, which means that this two-clamp system is capable of changing stiffness by a factor of 17. Moreover, when we compare the upper right triangle values and lower left triangle values of the stiffness matrix shown in Table 2, e.g., M1E0.05 and M0.05E1, which are 0.34 N/mm and 0.22 N/mm respectively, it is observed that the upper right triangle values are greater. Similarly, M0 column values are greater than E0 row values. These suggest that the middle clamp is more influential than the end clamp in changing stiffness.

2.6 Finite Element Analysis

To study the mechanical behavior of discrete layer jamming in more detail, a finite element (FE) model was built in ABAQUS with the same dimensions as the experimental setup shown in Table 1. Middle and end clamp pressures at combinations of 0, 0.01, 0.05, 0.1, 0.25, 0.5, 1, and 3 MPa for a total of 64 pressure states were simulated for 100 mm tip

Table 2 : Bending stiffness matrix from experiments.

Stiffness (N/mm)		Middle clamp pressure (MPa)				
		0	0.05	0.5	1	3
End clamp pressure (MPa)	0	0.024	0.12	0.17	0.17	0.17
	0.05	0.10	0.19	0.35	0.34	0.36
	0.5	0.11	0.22	0.39	0.40	0.40
	1	0.12	0.22	0.40	0.40	0.41
	3	0.11	0.19	0.39	0.39	0.40

deflection. C3D8I elements were used for meshing and NL-geom was turned on for large deformation. Small sliding and surface-surface contact were utilized to simulate contact conditions. The initial state of the simulation is shown in Fig. 2, and Fig. 7 shows the deflected shape for the M3E3 case. The deformation is not uniform due to buckling of the laminates. As a result, stresses concentrate at certain regions. One has to compare the maximum von Mises stress with material yield strength to determine whether the layers have plastically deformed. The resulting maximum von Mises stress is 30 MPa for the extreme case in Fig. 7, which is less than the yield strength of ABS (44 MPa). Since we expect a robotic arm to have much less deflection than 100 mm, the resulting von Mises stress will be much smaller than 44 MPa.

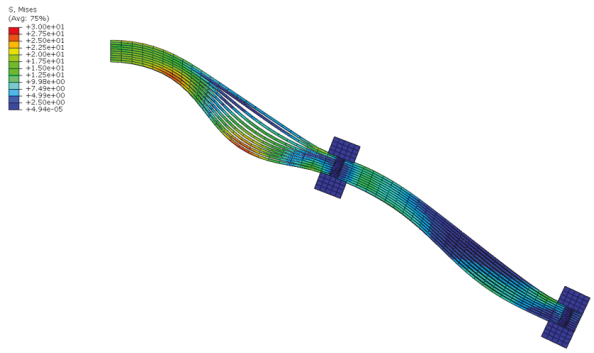

Fig. 7 : Resulting shape of M3E3 from FE simulation.

The force-displacement curves for 100 mm tip deflection at 5 representative pressure states are shown in Fig. 8(a). The curves are nonlinear but show linear behaviors for small deflections. It is observed that the curves for M0.5E0.5, M1E1, and M3E3 almost overlap, especially at small deflections, which indicates similar stiffness. Stiffness for each pressure state was obtained as the slope of the line fit for the first 20 mm of each force-displacement curve, as shown in Fig. 8(b).

2.7 Experiments vs. Simulations

Fig. 9 compares experimental and simulated stiffnesses, where "S" and "T" represent simulation and test, respectively. The simulation results agree with the experimental results very well except for the M0.05 series. This is because 0.05 MPa is a small load compared to the load cell range of 3.17 MPa. When we adjusted clamps between tests, some amount of variability was introduced to the applied clamp pressures, especially for lower pressure states, i.e., M0.05

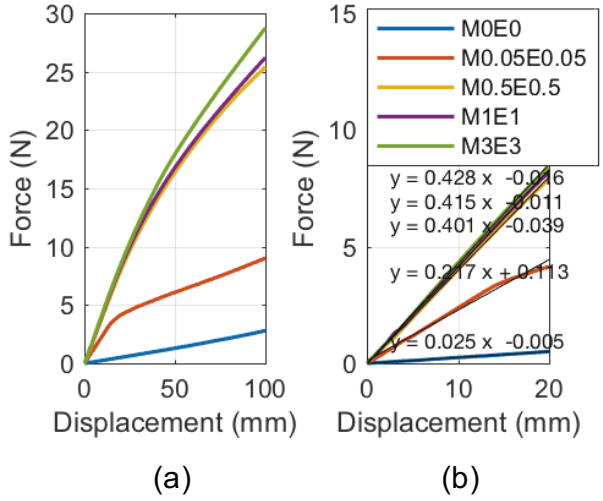

Fig. 8 : Force-displacement curves for 5 pressure states from FE simulations. (a) 100 mm displacement. (b) First 20 mm displacement with linear curve fits.

series. It is observed that the stiffness increases with the end clamp pressure. However, both experimental and simulation results indicate that pressures higher than 0.5 MPa will provide minimal increases in stiffness. From FEA, the maximum stiffness is obtained from M3E3 as 0.428 N/mm and the minimum stiffness is from M0E0 as 0.025 N/mm, which are comparable to 0.40 N/mm and 0.024 N/mm from experiments. The resulting maximum stiffness ratio from simulations is approximately 16.9, which is also in good agreement with the experimental result of 17. The overall agreement between FEA and experimental results validates the FEA model.

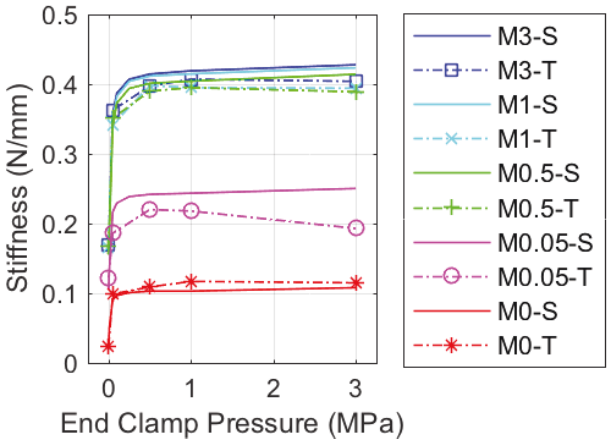

Fig. 9 : Comparison of stiffnesses from experiments and simulations, where "S" designates simulation results and "T" designates test results.

3 Computational Case Studies

In order to optimize the design of discrete layer jamming and develop a thorough understanding of how different design parameters affect bending stiffness, a series of computational case studies were developed and conducted. Key parameters of interest include clamp location, clamp width, number of laminates, friction coefficient and num-

ber of clamps. This section illustrates five case studies corresponding to these parameters that are investigated using ABAQUS simulations. For each parameter study, the specifications and results are summarized in one table.

3.1 Vary Middle Clamp Location

In the initial configuration discussed in the previous section, the first clamp was placed such that the beam was equally partitioned into two segments. In order to find out how the middle clamp location affects the stiffness of the structure, a case study was designed and carried out with simulations of various middle clamp locations. The setup for this case study is illustrated in Fig. 10. The length of the first segment is L_1, and the length ratio of the first segment to the full length is defined as $\alpha = L_1/L$. The length ratio α varies by eighths. All other dimensions are the same as those shown in Table 1. Two pressure states M0.05E0.05 and M3E3 are simulated for all middle clamp locations.

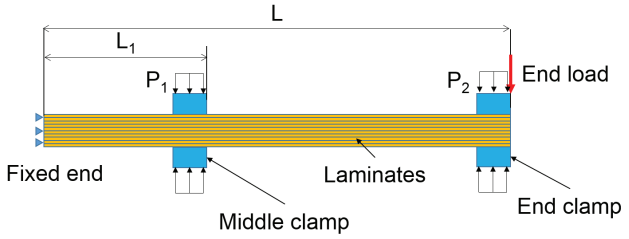

Fig. 10 : Schematic of configuration for middle clamp location case study.

Table 3 summarizes the resulting stiffness and maximum stiffness ratios K_r, where K_r is calculated as the ratio of stiffness of M3E3 at each clamp location over $k_{min} = 0.025$ N/mm, which corresponds to the clamp and pressure free state. Fig. 11 shows stiffness and stiffness ratio versus length ratio α for both M3E3 and M0.05E0.05 pressure states. It is observed that both curves are concave downward with a peak at $\alpha = 1/2$. Stiffness ratio has a maximum value of 16.9 at $\alpha = 1/2$ and minimum value of 6.1 at $\alpha = 7/8$. The concavity indicates that for this discrete layer jamming setup, the best location for the middle clamp is near the center of the beam, and the worst locations are near the ends of the beam.

Table 3 : Specifications and stiffness matrix for varying middle clamp location.

L_1 (mm)	50	100	150	200	250	300	350
α	1/8	1/4	3/8	1/2	5/8	3/4	7/8
Pressure (MPa)	Stiffness (N/mm)						
M0.05E0.05	0.117	0.159	0.203	0.217	0.211	0.177	0.131
M3E3	0.167	0.254	0.375	0.428	0.337	0.230	0.156
K_r	6.6	10.0	14.8	16.9	13.3	9.1	6.1

3.2 Vary Clamp Width

To study the effect of clamp width on beam stiffness, simulations with various clamp widths were performed. The setup for this case study is illustrated in Fig. 12. For simplification, the middle and end clamp widths were set to be equal. It was concluded in Section 3.1 that stiffness ratio is maximized when the middle clamp is positioned to partition the beam equally; therefore, that clamp location is used in this

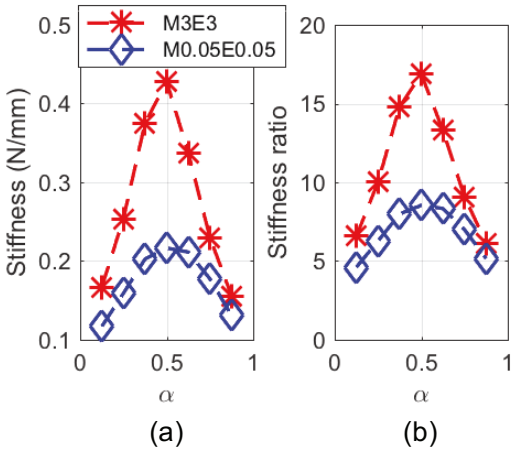

Fig. 11 : Stiffness trends for varying middle clamp location. (a) Stiffness versus length ratio. (b) Stiffness ratio versus length ratio.

study, where $L_1 = 200$ mm. Four different clamp widths have been studied including 10, 20, 40, and 80 mm. The pressures corresponding to the aforementioned clamp widths are set up as 6, 3, 1.5 and 0.75 MPa, which result in the same total clamping forces of 8400 N. All other specifications and dimensions are the same as those shown in Table 1. The clamping area ratio β is defined as the ratio of the sum of the clamp widths over the beam length for a beam with uniform width. For example, for a 400 mm long beam with two 20 mm wide clamps, β is calculated as $\beta = 2C/L = 2 * 20/400 = 0.1$. So, $\beta = 0$ corresponds to no clamping area, which is the minimum pressure state. All other dimensions are the same as those shown in Table 1.

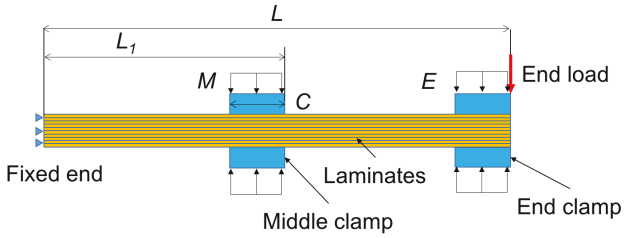

Fig. 12 : Schematic of configuration for clamp width case study.

Table 4 summarizes the resulting stiffness and maximum stiffness ratios K_r, where K_r is calculated as the ratio of stiffness at the specified pressure over $k_{min} = 0.025$ N/mm, which corresponds to the clamp and pressure free state. Stiffness and maximum stiffness ratio increase nonlinearly with β, as shown in Fig. 13. Maximum stiffness ratio increases to more than 40 when the clamps cover 40% of the area of the beam. It was also found that stiffness increases by a factor of 3.9 (from 0.260 N/mm to 1.025 N/mm) when the clamp width increases by a factor of 8 (from 10 mm to 80 mm). However, the increase of the stiffness comes not only from the increase in clamping area, but also the stiffness of the clamp. A large, stiff clamp may increase the quasi-static stiffness ratio but at the expense of adding bulk to the system, which is undesirable.

Table 4 : Specifications and stiffness matrix for varying clamp width.

C (mm)	0	10	20	40	80
β	0	0.05	0.1	0.2	0.4
Pressure (MPa)	0	M6E6	M3E3	M1.5E1.5	M0.75E0.75
Stiffness (N/mm)	0.025	0.260	0.428	0.562	1.025
K_r	1	10.3	16.9	22.2	40.4

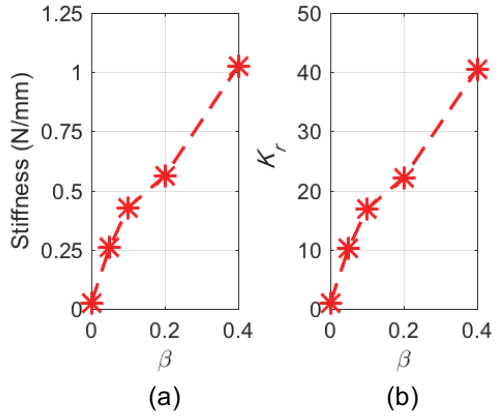

Fig. 13 : Stiffness trends for varying clamp width. (a) Stiffness versus clamping area ratio. (b) Maximum stiffness ratio versus clamping area ratio.

3.3 Vary the Number of Laminates

To study the effect of the number of laminates n on the stiffness of a structure, simulations with four different numbers were performed including 10, 5, 2, and 1, with laminate thicknesses selected to provide a total beam thickness of 15.875 mm. Here, $n = 1$ represents a beam with a single layer 15.875 mm thick. Four pressure states including the no pressure state, M0.05E0.05, M0.5E0.5, and M3E3 were simulated for all numbers of laminates. The minimum pressure state has no clamps or pressure. Also, there are no clamps or pressure applied for the case of $n = 1$, which has only a single laminate. While pressure does not affect the stiffness for this case, the results are shown at different pressure states for comparison. All other specifications and dimensions are the same as those shown in Table 1.

The stiffness varies nonlinearly with the number of laminates, as shown in Fig. 14. At each pressure state, the stiffness decreases with n and the stiffness ratio increases with n. Table 5 lists the resulting stiffnesses, maximum stiffness ratios K_r, and stiffness ranges. Here, K_r is calculated as the ratio of k_{max}/k_{min}, where k_{max} is the stiffness at M3E3 and k_{min} is the stiffness at the no pressure state for each number of laminates. The stiffness range was calculated as $k_{max} - k_{min}$ for each number of laminates. The state with no pressure or clamp applied has the smallest stiffness of 0.025 N/mm at $n = 10$ and the largest stiffness of 2.46 N/mm at $n = 1$, which is approximately 100 times that of former. This result agrees well with the theoretical maximum stiffness ratio n^2 for continuous layer jamming as discussed in Section 2.1. Even with only 5 layers, the maximum stiffness ratio is greater than 10. This may be a good design point for applications requiring both a high stiffness range and a high stiffness ratio. The highest maximum stiffness ratio of 16.9 is achieved with the highest number of laminates considered here ($n = 10$). The stiffness ratio can be further increased by reducing the laminate thickness and increasing the number of layers with the same total thickness. However, the minimum stiffness may be too low for robotic arm applications. The stiffness increases with decreasing n, regardless of the pressure state, which allows for a higher stiffness when a high stiffness ratio is not required. The highest stiffness range 1.533 N/mm is achieved with $n = 2$, which allows for both high stiffness and stiffness range, though its stiffness ratio is only 3.5.

Table 5 : Specifications and stiffness matrix for varying the number of laminates.

t (mm)	1.5875	3.175	7.9375	15.875
n	10	5	2	1
Pressure (MPa)	Stiffness (N/mm)			
No pressure	0.025	0.100	0.617	2.460
M0.05E0.05	0.217	0.282	0.687	2.460
M0.5E0.5	0.401	1.039	1.820	2.460
M3E3	0.428	1.170	2.150	2.460
Stiffness range (MPa)	0.403	1.07	1.533	0
K_r	16.9	11.7	3.5	1

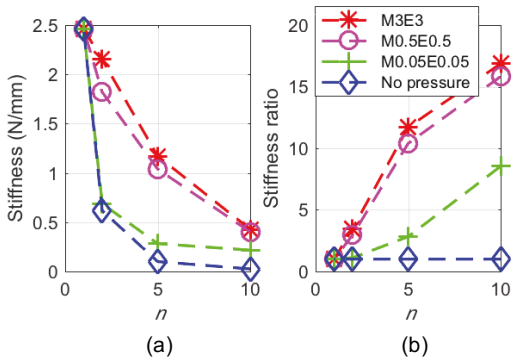

Fig. 14 : Stiffness trends for varying the number of laminates. (a) Stiffness versus the number of laminates. (b) Stiffness ratio versus the number of laminates.

3.4 Vary Laminate Friction Coefficient

This subsection presents simulation results to evaluate the effect of friction coefficient on discrete layer jamming. The simulations were conducted with seven friction coefficients including 0.15, 0.3, 0.45, 0.6, 0.9, 1.2, and 2. For every friction coefficient μ, four pressure states were simulated including no pressure, M0.05E0.05, M0.5E0.5, and M3E3. The no pressure state does not include clamps and is the minimum pressure state. All other specifications and dimensions are the same as those shown in Table 1.

Table 6 lists some of the results in detail. The maximum stiffness ratio K_r was calculated as the stiffness at M3E3 pressure state over k_{min} for each friction coefficients, where k_{min} corresponds to the stiffness with no pressure or clamp.

Both Fig. 15 and Fig. 16 show the effects of friction on stiffness and stiffness ratio: Fig. 15 shows the trends of stiffness and stiffness ratio with respect to friction coefficient at different pressure states; Fig. 16 shows the curves of stiffness and stiffness ratio versus pressure states for different friction coefficients. Fig. 15 shows that the stiffness increases with friction coefficient, though the magnitude of the effect is different for different pressure states. Friction coefficient has little effect on bending stiffness at the no pressure state due to the lack of friction force. However, friction coefficient

Table 6 : Specifications and stiffness matrix for varying friction coefficient.

μ	0.15	0.45	0.6	1.2	2
Pressure (MPa)	Stiffness (N/mm)				
No pressure	0.025	0.025	0.025	0.026	0.027
M0.05E0.05	0.093	0.182	0.217	0.296	0.344
M0.5E0.5	0.341	0.392	0.401	0.419	0.431
M3E3	0.418	0.425	0.428	0.436	0.445
K_r	16.9	16.9	16.9	16.8	16.7

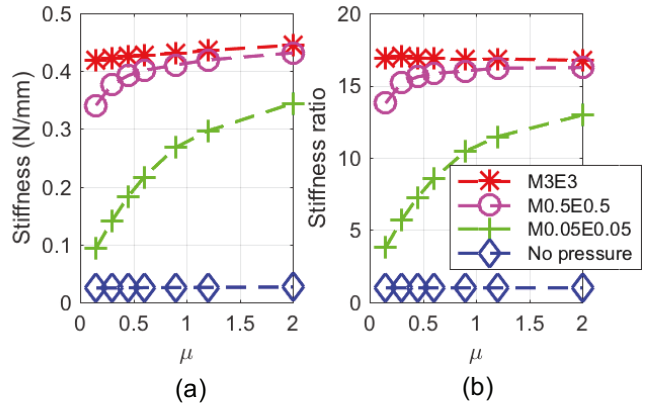

Fig. 15 : Stiffness trends for varying friction coefficient. (a) Stiffness versus friction coefficient. (b) Stiffness ratio versus friction coefficient.

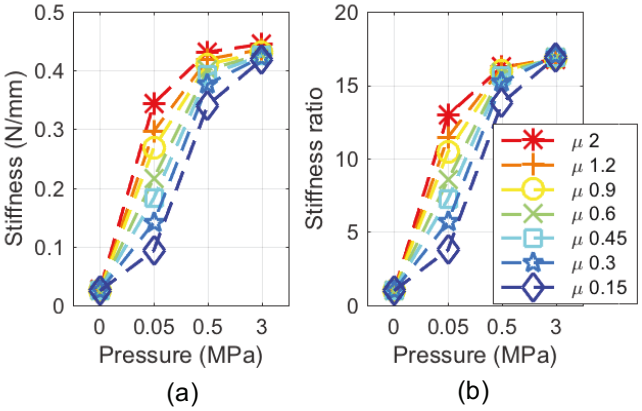

Fig. 16 : Stiffness trends for varying friction coefficient. (a) Stiffness versus pressure. (b) Stiffness ratio versus pressure.

has a much greater effect on bending stiffness for low pressure states than high pressure states. For example, increasing the friction coefficient from $\mu = 0.15$ to $\mu = 2$ increases the stiffness by 270% (0.093 N/mm to 0.344 N/mm) at the M0.05E0.05 state but only 6% (0.418 N/mm to 0.445 N/m) for the M3E3 state. Despite the effect of friction coefficient on stiffness, maximum stiffness ratios K_r were found to be almost the same for all friction coefficient cases. At the highest pressures considered here, e.g., M0.5E0.5 and M3E3, the friction coefficient has little effect on the stiffness. The stiffness for $\mu = 2$ at M0.05E0.05 and $\mu = 0.15$ at M0.5E0.5 are almost the same, which is consistent with (2), since the friction force can be increased by increasing either the friction coefficient or the clamping pressure.

In addition, Fig. 16 shows that the stiffness and stiffness ratio versus pressure curves exhibit different shapes for different μ: lower friction coefficient curves such as $\mu = 0.15$ exhibit S-shaped curves; higher friction coefficient curves such as $\mu = 2$ show sharp slopes at lower pressure states, i.e., from the no pressure state to M0.05E0.05, followed by mild slopes at higher pressure states. These provide valuable guidelines for design and actuation requirements. Smaller friction coefficients can help achieve smoother transition of stiffness when used with high force actuators. Higher friction coefficients are needed if the actuation force is limited and a high maximum stiffness ratio is required.

3.5 Vary the Number of Clamps

This subsection presents simulation results to identify the effect of the distribution of the clamping force (i.e., number of clamps) on discrete layer jamming. The simulations were conducted with four different numbers of clamps N as 1, 2, 3 and 4, as shown in Fig. 17. The corresponding single clamp widths are 40, 20, 40/3, and 10 mm, respectively. Hence the total clamping area is kept constant, with the clamp widths adding up to 40 mm for all cases. The same pressure of 3 MPa is applied to all clamps and cases so that the total clamping force is the same (8400 N) for each case. Considering the application of a robot manipulator which requires a stiff end for the payload, we simulated the one clamp setup with the only clamp placed at the end, as shown in Fig. 17(a). For the other cases, the clamps were distributed equally to partition the beam into 2, 3, and 4 segments. All other specifications and dimensions are the same as those shown in Table 1.

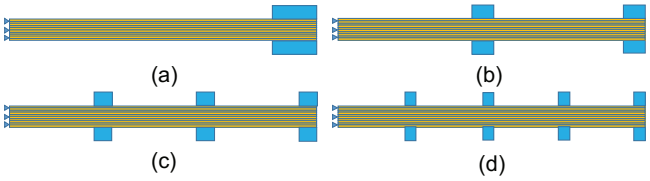

Fig. 17 : Schematic of configurations for the number of clamps case study. (a) One clamp with single clamp width of 40 mm. (b) Two clamps with single clamp width of 20 mm. (c) Three clamps with single clamp width of 40/3 mm. (d) Four clamps with single clamp width of 10 mm.

Fig. 18 and Table 7 illustrate the relationship between the stiffness and number of clamps. Maximum stiffness ratios K_r, as shown in Table 7, are calculated as the ratio of stiffness for each number of clamps at 3 MPa (except N=0 case, no clamps or pressure state) over $k_{min} = 0.025$ N/mm, which corresponds to the clamp and pressure free state. Both stiffness and maximum stiffness ratio were found to increase drastically with an increasing number of clamps. The stiffness increases by approximately a factor of 3 from 0.428 N/mm to 1.167 N/mm when the number of clamps increases from 2 to 4. The key reason is that the distribution of the clamps delays the onset of layer buckling , which can be observed in Fig. 7 as well as in Fig. 5. With four clamps distributed equally, simulations indicate a maximum stiffness ratio of 46. Considering that the clamps only apply pressure to 10% of the length of the beam, this is fairly high compared to the theoretical limit of 100 for continuous layer jamming, which requires covering the full length of the beam. It can be extrapolated that distributing of the clamping force over

more clamps may produce higher stiffness ratios. While this would require more actuators, since a lower clamping force is needed to achieve the same pressure for narrower clamps, smaller, lower-force actuators could be used.

Table 7 : Specifications and stiffness matrix for varying the number of clamps.

N	0	1	2	3	4
Single clamp width (mm)	0	40	20	40/3	10
Pressure (MPa)	0	3	3	3	3
Stiffness (N/mm)	0.025	0.122	0.428	0.821	1.167
K_r	1.0	4.8	16.9	32.4	46.0

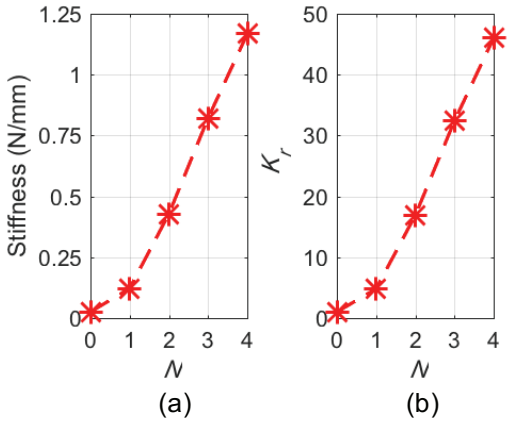

Fig. 18 : Stiffness trends for varying the number of clamps. (a) Stiffness versus the number of clamps. (b) Maximum stiffness ratio versus the number of clamps.

3.6 Summary of Computational Case Studies

In this subsection, the effects of different discrete layer jamming design parameters on beam stiffness properties are discussed and summarized.

In Section 2.1, both experimental and computational studies were presented that investigated the effect of clamping pressure on beam bending stiffness. From the experiments, it was found that the stiffness increases with pressure for both clamps. A 16.9 times stiffness increase was achieved with the current simulation setup and range of pressures tested. Because increasing pressure primarily serves to delay the onset of laminate slipping, further increasing the pressure has little effect on the stiffness for small deflections. The simulation and experimental results were in good agreement, thus validating the finite element model that was used for the case studies presented in this section.

In Section 3.1, we showed that positioning the middle clamp to form equal partitions of the beam yields the largest stiffness and maximum stiffness ratio. For more than two clamps, further FE simulation or analytical modeling would be required to determine the optimal distribution of the clamps.

In Section 3.2, increasing clamp area for a given force was shown to significantly increase the stiffness and stiffness ratio. With 40% of the length of a beam clamped, a 40.4 times increase in stiffness can be achieved. Large clamps will increase the weight of the whole structure, which is not desirable. However, with just 10% of the length of the beam clamped as what we set up in our experimental studies, 16.9 times stiffness increase was realized.

Section 3.3 compares the stiffness ratios for beams with different numbers of laminates but the same total thickness. It was found that with more, thinner laminates, higher stiffness ratios can be achieved. However, the minimum stiffness may be inefficient for robotic arm applications, and beams with thinner laminates require a higher pressure to actuate a stiff state.

The effect of friction coefficient was studied in Section 3.4. It was found that higher friction coefficient yields higher stiffness and stiffness ratio at lower pressure states, though it has little effect on stiffness or stiffness ratio at higher pressure states, e.g., maximum stiffness or maximum stiffness ratio. For example, increasing the friction coefficient from 0.15 to 2 only increases the maximum stiffness from 0.418 N/mm to 0.445 N/mm, and the maximum stiffness ratio decreases from 16.9 to 16.7. Increasing the friction coefficient has an equivalent effect as increasing the clamp pressure, which both serve to increase the friction force between layers as we observed in (2). High friction force cases show similar stiffness, which again indicates that increasing friction force primarily serves to delay the onset of laminate slipping, so further increasing the friction force has little effect on the stiffness for small deflections.

Section 3.5 shows the effect of varying the number of clamps with the same total clamp width on stiffness. The key finding is that the stiffness increases drastically with the number of clamps: increasing the number of clamps from 2 to 4 increases the maximum stiffness ratio from 17 to 46. This is promising compared to vacuum-based continuous layer jamming which can theoretically achieve a 100 times maximum stiffness ratio but requires an exterior membrane and a pneumatic source.

All parameters affect the beam bending stiffness and stiffness ratio. Parameters except friction coefficient affect the maximum stiffness ratio significantly within the pressure range investigated. Increasing clamp area and number of clamps can likely be extrapolated to slightly larger clamping areas and distributions of clamps, but the concept of discrete layer clamping loses its practicality for very large numbers of clamps or very large clamping areas. In those cases, alternative jamming mechanisms such as pneumatic vacuum probably is more appropriate. Therefore, the two remaining parameters, clamp location and number of laminates, are most useful for optimizing a discrete layer jamming design with constraints for clamp area and number of clamps.

4 Actuation Requirements

To quantify the actuation requirements for a variable pressure clamp, quasi-static compression tests were set up and performed on a stack of 10 ABS layers. Specifications for the ABS layers and the experimental setup are shown in Table 1 and Fig. 19, respectively. Clamping force was applied by an aluminum mechanical clamp with a width of 20

mm. Five random locations (samples) along the beam were tested 3 times each for a total of 15 tests. For each test, the clamp was loaded to 15 kN, corresponding to a clamping pressure of 10.71 MPa. The tests were conducted with a loading rate of 0.02 mm/s. The compression force and displacement were measured by an MTS load frame at a sampling rate of 10 Hz.

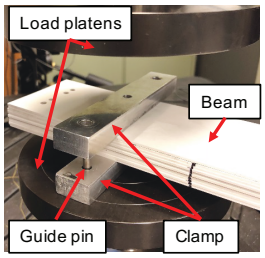

Fig. 19 : Beam compression test setup.

We processed the data from the beam compression tests by: (1) at each load level, subtracting the corresponding displacement per the load frame compliance relationship obtained from load frame compression tests, (2) smoothing the curve with a moving average filter with a span of 5 and removing data points with force less than 1 N to compensate for signal noise, (3) the first point with force equal to or greater than 1 N among the remaining data points are defined as the starting point for each force-displacement curve. An averaged force-displacement curve was obtained by averaging the displacements at each load level. The processed force-displacement curves and the average curve are shown in Fig. 20(a) and Fig. 20(b), respectively. The curves in Fig. 20(a) are labeled as T_{ij}, where i indicates the location number and j the measurement number. From Section 2 we found that increasing pressure higher than 0.5 MPa provides a negligible increase in stiffness or stiffness ratio, so 0.5 MPa is a reasonable requirement for actuation force. With a safety factor of 1.2, we may select 0.6 MPa as a final maximum actuation pressure target. For a clamping area of 20 mm x 70 mm, a maximum actuation force of 840 N is needed. The stroke required at 840 N was obtained from the average force-displacement curve as 0.332 mm, and the targeted clamp force-displacement is indicated by a red circle in Fig. 20(b). For reference, a blue dot corresponding to a clamping force of 4200 N (pressure of 3 MPa) and a displacement of 0.381 mm is also shown in Fig. 20(b). This illustrates that increasing the force by a factor of 5 requires only 15% more stroke.

Therefore, our targeted maximum actuation force and stroke are 840 N and 0.332 mm, respectively. Other actuator requirements including size, weight, and actuation speed are highly dependent on the robot application and specific manipulator design.

5 Conclusions

This paper has introduced a discrete layer jamming mechanism to achieve tunable stiffness. Design, computational (FE) modeling, analysis, and experimental results of

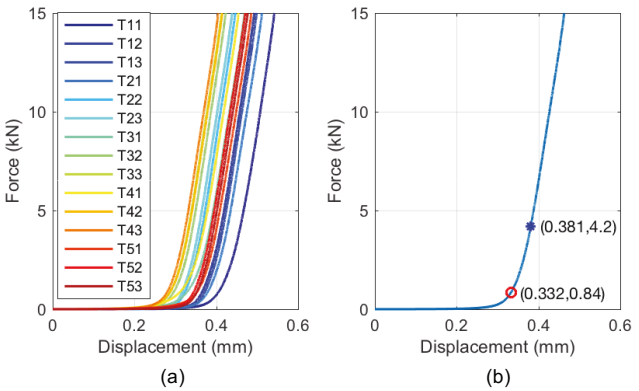

Fig. 20 : Compression test force-displacement data for 5 samples with 3 tests each for a force threshold of 1 N. (a) The processed curves. (b) Average curve.

variable stiffness discrete jamming beam structures were presented. Both simulations and experiments verified that beam bending stiffness increases with clamp pressure. Computational case studies showed that the beam stiffness also depends on the number of layers, clamp width, clamp location, friction coefficient, and the number of clamps.

Compared to pneumatic continuous layer jamming, the external surface of the discrete layer jamming method does not require an elastomeric membrane, and is therefore less likely to be damaged due to accidental impact or contact with rough edges. The discrete jamming structure can be used as a manipulator for co-robots to improve safety by reducing stiffness during fast travel and stiffening for final positioning accuracy.

Further efforts should include the development of analytical models to describe the relationship between pressure and bending stiffness. With these models, smart material clamps with fast response and high clamping pressure will be investigated and developed. Flextensional piezoelectric actuators and shape memory alloy wire strips with heat insulation for actuation are under consideration. Further analytical modeling and analysis of interlaminar friction would enable more precise stiffness control.

Acknowledgements

This research is supported by the National Science Foundation, National Robotics Initiative Grant No: CMMI-1637656.

References

[1] Frisoli, A., Rocchi, F., Marcheschi, S., Dettori, A., Salsedo, F., and Bergamasco, M., 2005. "A new force-feedback arm exoskeleton for haptic interaction in virtual environments". In Eurohaptics Conference, 2005 and Symposium on Haptic Interfaces for Virtual Environment and Teleoperator Systems, 2005. World Haptics 2005. First Joint, IEEE, pp. 195–201.

[2] Roderick, S., and Carignan, C., 2007. "Designing

safety-critical rehabilitation robots". In *Rehabilitation Robotics*. InTech.

[3] Wolbrecht, E. T., Chan, V., Reinkensmeyer, D. J., and Bobrow, J. E., 2008. "Optimizing compliant, model-based robotic assistance to promote neurorehabilitation". *IEEE Transactions on Neural Systems and Rehabilitation Engineering,* **16**(3), pp. 286–297.

[4] Krüger, J., Lien, T. K., and Verl, A., 2009. "Cooperation of human and machines in assembly lines". *CIRP Annals-Manufacturing Technology,* **58**(2), pp. 628–646.

[5] She, Y., Su, H.-J., Meng, D., Song, S., and Wang, J., 2018. "Design and modeling of a compliant link for inherently safe corobots". *Journal of Mechanisms and Robotics,* **10**(1), p. 011001.

[6] Bicchi, A., and Tonietti, G., 2004. "Fast and "soft-arm" tactics [robot arm design]". *IEEE Robotics & Automation Magazine,* **11**(2), pp. 22–33.

[7] Tonietti, G., Schiavi, R., and Bicchi, A., 2006. "Optimal mechanical/control design for safe and fast robotics". In *Experimental Robotics IX*. Springer, pp. 311–320.

[8] Chen, L., Garabini, M., Laffranchi, M., Kashiri, N., Tsagarakis, N. G., Bicchi, A., and Caldwell, D. G., 2013. "Optimal control for maximizing velocity of the compact^{TM} compliant actuator". In Robotics and Automation (ICRA), 2013 IEEE International Conference on, IEEE, pp. 516–522.

[9] Garabini, M., Passaglia, A., Belo, F., Salaris, P., and Bicchi, A., 2011. "Optimality principles in variable stiffness control: The vsa hammer". In Intelligent Robots and Systems (IROS), 2011 IEEE/RSJ International Conference on, IEEE, pp. 3770–3775.

[10] Stilli, A., Grattarola, L., Feldmann, H., Wurdemann, H. A., and Althoefer, K., 2017. "Variable stiffness link (vsl): Toward inherently safe robotic manipulators". In Robotics and Automation (ICRA), 2017 IEEE International Conference on, IEEE, pp. 4971–4976.

[11] She, Y., Su, H.-J., Lai, C., and Meng, D., 2016. "Design and prototype of a tunable stiffness arm for safe human-robot interaction". In ASME 2016 International Design Engineering Technical Conferences and Computers and Information in Engineering Conference, American Society of Mechanical Engineers, pp. V05BT07A063–V05BT07A063.

[12] She, Y., Meng, D., Cui, J., and Su, H.-J., 2017. "On the impact force of human-robot interaction: Joint compliance vs. link compliance". In Proceedings of IEEE 2017 International Conference on Robotics and Automation (ICRA).

[13] Amend, J. R., Brown, E., Rodenberg, N., Jaeger, H. M., and Lipson, H., 2012. "A positive pressure universal gripper based on the jamming of granular material". *IEEE Transactions on Robotics,* **28**(2), pp. 341–350.

[14] Ranzani, T., Cianchetti, M., Gerboni, G., De Falco, I., and Menciassi, A., 2016. "A soft modular manipulator for minimally invasive surgery: design and characterization of a single module". *IEEE Transactions on Robotics,* **32**(1), pp. 187–200.

[15] Wei, Y., Chen, Y., Yang, Y., and Li, Y., 2016. "A soft robotic spine with tunable stiffness based on integrated ball joint and particle jamming". *Mechatronics,* **33**, pp. 84–92.

[16] Tabata, O., Konishi, S., Cusin, P., Ito, Y., Kawai, F., Hirai, S., and Kawamura, S., 2001. "Micro fabricated tunable bending stiffness devices". *Sensors and Actuators A: Physical,* **89**(1-2), pp. 119–123.

[17] Henke, M., and Gerlach, G., 2014. "On a high-potential variable-stiffness device". *Microsystem technologies,* **20**(4-5), pp. 599–606.

[18] Follmer, S., Leithinger, D., Olwal, A., Cheng, N., and Ishii, H., 2012. "Jamming user interfaces: programmable particle stiffness and sensing for malleable and shape-changing devices". In Proceedings of the 25th annual ACM symposium on User interface software and technology, ACM, pp. 519–528.

[19] Santiago, J. L. C., Walker, I. D., and Godage, I. S., 2015. "Continuum robots for space applications based on layer-jamming scales with stiffening capability". In Aerospace Conference, 2015 IEEE, IEEE, pp. 1–13.

[20] Kim, Y.-J., Cheng, S., Kim, S., and Iagnemma, K., 2013. "A novel layer jamming mechanism with tunable stiffness capability for minimally invasive surgery". *IEEE Transactions on Robotics,* **29**(4), pp. 1031–1042.

[21] Zhu, M., Mori, Y., Xie, M., Wada, A., and Kawamura, S., 2018. "A 3d printed two dof soft robotic finger with variable stiffness". In 2018 12th France-Japan and 10th Europe-Asia Congress on Mechatronics, IEEE, pp. 387–391.

[22] Choi, W. H., Kim, S., Lee, D., and Shin, D., 2019. "Soft, multi-dof, variable stiffness mechanism using layer jamming for wearable robots". *IEEE Robotics and Automation Letters,* **4**(3), pp. 2539–2546.

[23] Bamotra, A., Walia, P., Prituja, A. V., and Ren, H., 2019. "Layer-jamming suction grippers with variable stiffness". *Journal of Mechanisms and Robotics,* **11**(3), p. 035003.

[24] Zhou, Y., Headings, L. M., and Dapino, M. J., 2019. "Discrete layer jamming for safe co-robots". In Proceedings of IEEE 2019 International Conference on Robotics and Automation (ICRA).

[25] Kawamura, S., Yamamoto, T., Ishida, D., Ogata, T., Nakayama, Y., Tabata, O., and Sugiyama, S., 2002. "Development of passive elements with variable mechanical impedance for wearable robots". In Robotics and Automation, 2002. Proceedings. ICRA'02. IEEE International Conference on, Vol. 1, IEEE, pp. 248–253.